Chemical and Process Engineering 2022, 43 (3), 331–355
DOI: 10.24425/cpe.2022.142278

CFD MODELING OF DROPLET GENERATION PROCESS FOR MEDICAL APPLICATIONS USING THE ELECTROSTATIC IMPULSE METHOD

Piotr Cendrowski[1], Katarzyna Kramek-Romanowska[1], Dorota Lewińska[2], Marcin Grzeczkowicz[2], Paulina Korycka[3], Jan Krzysztoforski[1]*

[1]Warsaw University of Technology, Faculty of Chemical and Process Engineering, Ludwika Waryńskiego 1, Warsaw, Poland

[2]Nalecz Institute of Biocybernetics and Biomedical Engineering Polish Academy of Sciences, Ks. Trojdena 4, Warsaw, Poland

[3]Foundation of Research and Science Development, Rydygiera 8, 01-793 Warsaw, Poland

The electrostatic impulse method is an established method for producing microbeads or capsules. Such particles have found application in biomedical engineering and biotechnology. The geometric properties of the droplets – constituting precursors of microbeads and capsules – can be precisely controlled by adjusting the geometry of the nozzle system, the physical properties and the flow rate of the fluids involved, as well as the parameters of the electrostatic impulse. In this work, a method of mathematical modeling of the droplet generation process using the electrostatic impulse method in a single nozzle system is presented. The developed mathematical model is an extension of the standard Volume of Fluid (VOF) model by addition of the effect of the electric field on the fluid flow. The model was implemented into the OpenFOAM toolkit for computational fluid dynamics (CFD). The performed CFD simulation results showed good agreement with experimental data. As a result, the influence of all process parameters on the droplet generation process was studied. The most significant change in droplet generation was caused by changing the electrostatic impulse strength. The presented modeling method can be used for optimization of process design and for studying the mechanisms of droplet generation. It can be extended to describe multi nozzle systems used for one-step microcapsule production.

Keywords: droplet generation, electrostatic impulse method, encapsulation, CFD, OpenFOAM

1. INTRODUCTION

Encapsulation is a process with constantly growing number of applications in various fields of science and technology, including food industry (Madene et al. 2006; Shahidi and Han, 1993), analytical chemistry (Papadimitriou et al., 2020), biotechnology (Betancor and Luckarift, 2008; Köster et al., 2008; Pierre, 2004; Yaakov et al., 2018) and biomedical engineering (Krishnan et al., 2014; Vaithilingam and Tuch, 2011). There are several methods of creating capsules – using chemical reactions and physical processes, some of them including the use of an electric field (Prüsse et al., 2008). Depending on the final application of the capsule, various requirements regarding the size, shape, composition have to be met. Especially

* Corresponding author, e-mail: jan.krzysztoforski@pw.edu.pl

in biomedical applications of encapsulation processes, where living cells are encapsulated, many factors, including the geometry of the capsules, hydrodynamic stresses during the production process, nutrition of the cells, reduction of the immune response, have to be considered (Hu and de Vos, 2019; Hunkeler et al., 2001; Krishnan et al., 2014; Hyerim et al., 2019; Lewińska et al., 2008; Vaithilingam and Tuch, 2011; Zhang and He, 2009). These requirements impose the need of extensive study of materials, devices and operational conditions used in encapsulation process.

It has already been over 60 years, since TMS Chang presented his ingenious idea of "artificial cells": erythrocytes surrounded by a polymer membrane that would play the role of "blood substitute". This is the concept underlying the area of research that has been rapidly developing for the past 20 years and is related to nanomedicine, drug delivery systems, enzyme/gene therapy, cell/stem cell therapy, bioencapsulation, cell encapsulation/scaffold, regenerative medicine, nanobiotechnology and many other areas of advanced science including biomedical engineering (Chang 2019).

Immobilization and encapsulation of biologically active material is defined by the UPAC (Union of Pure and Applied Chemistry) as follows (IUPAC, 1997): "enzymes or cells which are of relatively large size may be entrapped in a maze of polymeric molecules (a gel). This procedure is called immobilization by inclusion. When the biocatalyst is enclosed inside a semipermeable membrane, usually approximately spherical, the method is known as encapsulation". These are two of the basic techniques that are being intensively developed, researched and applied in modern biotechnology, pharmacy, experimental medicine, and biomedical engineering.

Encapsulation of drugs (Ferreira et al. 2015; Ganesh et al., 2018; Vakilinezhad et al., 2018), bioactive proteins, peptides such as enzymes (Betancor and Luckarift, 2008; Zhai et al., 2015), hormones (Baskaran et al., 2018; Cárdenas-Bailón et al., 2015), cellular growth factors (Osswald and Kang-Mieler, 2016), vaccine candidates (Anugraha et al., 2015) and many others is usually done using emulsion methods (water/oil/water type), often combined with solvent evaporation, spray-drying, freeze-drying (Shahidi and Han, 1993) or surfactant organized interfacial complexation (Duan et al., 2018). These methods allow the formation of micro- (Yaakov et al., 2018) and nanoparticles, which raises the therapeutic effectiveness of encapsulated materials. On the one hand, this protects them from adverse environmental impact that causes their degradation (pH, temperature, oxidants) and simultaneously increases their bioavailability, allowing their direct delivery to the location of therapeutic action (e.g., via an injection directly into a cancerous tumor (Vakilinezhad et al., 2018)). A particularly advantageous method of preparing homogeneous emulsions is the microfluidic technique (in which the dispergation phase takes the form of droplets that are homogeneous in terms of size, with a diameter from several hundred nanometers to several hundred micrometers) (Eberhardt et al., 2019; Köster et al., 2008) used mainly to analyze samples on a micro scale via lab-on-a-chip type devices (Papadimitriou et al., 2020).

The problem of maintaining stability of the encapsulated material is particularly important in the case of orally delivered proteins (Cárdenas-Bailón et al., 2015) and functional food ingredients (Manjula and Bhagath, 2017; Picot et al., 2015) due to the adverse conditions in the digestive tract that contribute to the loss of the bioactive properties of the encapsulated material.

The emulsion method, though cheap and easy to conduct, when applied on an industrial scale, is not appropriate for encapsulation of live cells because it requires the use of toxic solvents. To that end, the two-stage method known since 1980 and proposed by Lim and Sun (1980) for encapsulation of pancreatic islets can be used. In the first stage, a hydrogel microsphere is formed, which is then coated, via successive baths in polymer solutions with an opposing charge, in successive layers of polymer, creating a semi-permeable membrane. The core of the sphere is formed by a spherical hydrogel matrix that contains the encapsulated cells. It is usually composed of biocompatible alginate cross-linked by calcium ions. This method is used to immobilize live cells including probiotics (Liu et al., 2019), microbial cells (Rathore et al., 2013) and microbial biological control agents (Vemmer and Patel, 2013). To ensure that encapsulated

cells have the best possible conditions for survival and multiplication, the gel microsphere should have the smallest possible diameter: below 200 μm (Zhang and He, 2009). To meet this requirement cells are immobilized using methods that assure their safety: extrusion combined with simultaneous separation of the stream of the cell suspension extruded through a narrow nozzle using various means (Lewińska et al., 2008): coaxial air-flow, vibration, jet-cutter (Prüsse et al., 2008) or electrostatic method (Bugarski et al., 1994; Poncelet et al., 1994). Increasingly more often, particularly in case of encapsulation of single cells such as stem cells, a method involving microfluidic encapsulation in droplets is used.

In the case of encapsulation of live cells for therapeutic purposes in the form of implants, it is necessary to cover the microsphere containing the cells in a semi-permeable membrane, usually formed from polycations such as poly-L-lysine, polyornithine or poly(methyl-co-guanidine) (Bhatia et al., 2005). The task of the membrane is to protect encapsulated cells against destruction by the recipient's immune system, i.e. immunisolation (de Vos, 2017), which is necessary in the case of xenotransplantation. Correct functioning of implanted cells is directly dependent on biocompatibility of the capsule-cell-recipient system and for this reason, it has been intensively studied with respect to the purity of the materials used (Hu and de Vos, 2019), the way encapsulation is conducted (Krishnan et al., 2014; Vaithilingam et al., 2011; Vaithilingam and Tuch, 2011), the sources and means of obtaining cells (Hunkeler et al., 2001).

One of the increasingly popular methods of immobilizing biologically active substances (including natural and genetically modified cells (Diel et al., 2018)) in gel microspheres is the electrostatic method proposed by Bugarski and Poncelet (Bugarski et al., 1994). It uses the phenomenon of decreasing surface tension of a liquid extruded through a thin metal nozzle located in an electrostatic field (Castellanos, 1998). The diameter of microdroplets formed with the electrostatic method, both classic (in a constant field (Cárdenas-Bailón et al., 2015)) and impulse (Lewińska et al., 2008), is strongly dependent on the diameter of the nozzle, process parameters (for example the voltage applied) (Goosen et al., 1997), the rheological properties of the liquid used to form the microdroplets (Kramek-Romanowska et al., 2019; Manojlovic et al., 2006), where an impulse field is used, also the frequency and duration of the electrical impulses (Lewińska et al., 2004). These relationships may be observed as well when a double (Lewińska et al., 2008) and a triple (Lewińska et al., 2012) coaxial head is used. In this situation, given such a large number of parameters impacting the size and size homogeneity of the microdroplets formed, the advantageous solution is to optimize this technique using numerical methods for fluid flow simulation. Similar challenges have been identified in other practical applications of charged droplets of liquids, such as conversion of the kinetic energy of accelerated, electrically charged droplets into electrical energy (Xie et al., 2014), development of electrostatic transducers (Allegretto et al., 2018), sorting by diameter in microfluidic systems (Ahn et al., 2009) and the drop-on-demand 3D printing technique (Plog et al., 2020).

Computational fluid dynamics (CFD) is a widely used tool for numerical investigation of complex flow systems involving droplets, e.g. devices for droplet generation (Chaves et al., 2020) and emulsification (Kobayashi et al., 2011). The Navier–Stokes equation, representing the momentum balance, can be solved together with the Maxwell equations in order to study electrohydrodynamics (EHD) (Castellanos, 1998) or magnetohydrodynamics (MHD) (Rakoczy et al., 2021). CFD was applied successfully to model complex flow systems for droplet generation, in various works, including the influence of electric forces on fluid flow. For example, Roghair et al. (2015) developed a numerical model to simulate the behavior of display pixels – the aim of their work was to study dynamics of electrowetting-based pixels. Good agreement with experimental work was achieved, while still acknowledging some room for improvement. Wu et al. (2017) applied CFD to model electrohydrodynamic jet printing. A model was created, which can be used to describe the printing with more than just the empirical approach, and which is a starting point toward a precise tool, which could allow to test the process parameters in quick and easy manner. Another work utilizing CFD was published by Lastow and Balachandran (2006). Their idea was to collect the previous works on atomization into one comprehensive theory. The created model contained EHD and electrostatic equations. Results were compared against experimental work and qualitative agreement was achieved.

Darabi and Rhodes (2006) created a numerical model for simulating work of ion-drag EHD pump. It was then tested against experimental data – using the operational parameters which were found to be the best, according to the simulation. The agreement of experimental and numerical data was good and acquired model allows numerical optimization of process. Li and Zhang (2020) performed extensive work on naming different flow regimes for droplet generation processes. Thanks to their numerical modeling, it is possible to design process parameters to acquire desired outcome. Xia and Reboud (2019) ran an extensive set of experiments on the process of electrostatic droplet generation and electrocoalescence. Furthermore, they compared experimental results with mathematical modeling. Good agreement between those two approaches was obtained, which validates this method for use in dehydration of oil-water emulsions. Wei et al. (2013) carried out investigation of cone jet formation and electrostatic spray. Possible process outcomes and factors were carefully investigated and described. As a result, a physical model was proposed and validated. Rahman et al. (2010) investigated droplet generation through electrostatic forces, aiming at improving the process for purpose of electrostatic inkjet printing. Numerical simulations were carried out and tested against experimental data. Qualitative but not quantitative agreement was reached and some general trends for the process were described. In these studies, various types of CFD simulation software were used, including the open-source CFD toolbox OpenFOAM (Roghair et al., 2015; Wei et al., 2013; Wu et al., 2017).

The aim of this work was to develop a mathematical model suitable for CFD modeling of droplet generation process using the electrostatic impulse method. The developed model should provide better understanding of the investigated process and allow to run numerical experiments with almost every combination of operational parameters (e.g. nozzle diameter, strength and frequency of oscillation of electrical field, viscosity and density of fluids, mass flow rate of liquid). Moreover, the model proposed in this work is regarded as the first step of the development of a modeling method for the encapsulation process using multi-nozzle systems (Lewińska et al., 2012).

2. MATERIALS AND METHODS

2.1. Mathematical model

In this work, the Volume of Fluid (VOF) multiphase flow model for incompressible fluids was extended by terms and equations representing the influence of the electric field on fluid flow (Tomar et al., 2007; Hirt and Nichols, 1981; López-Herrera et al., 2011; Roghair et al., 2015). The model was developed analogically to the work by Roghair et al. (2015). The equations of the model are listed below:

Continuity equation (overall mass balance for incompressible fluid flow):

$$\nabla \cdot \boldsymbol{U} = 0 \tag{1}$$

where $\boldsymbol{U}$ is the velocity of fluid.

Change of volume fraction (mass balance):

$$\frac{\partial \alpha}{\partial t} + \nabla \cdot (\boldsymbol{U}\alpha) = 0 \tag{2}$$

where α is the volume fraction of the liquid phase, $\boldsymbol{U}$ – fluid velocity, and t – time.

Momentum balance (Navier–Stokes equation for incompressible fluid flow):

$$\rho\left(\frac{\partial \boldsymbol{U}}{\partial t} + \boldsymbol{U} \cdot \nabla \boldsymbol{U}\right) = -\nabla p + [\nabla \cdot (\mu \nabla \boldsymbol{U})] + \boldsymbol{F_g} + \boldsymbol{F_\sigma} + \boldsymbol{F_E} \tag{3}$$

Density and viscosity are calculated as weighted averages:

$$\rho = \rho_1 \alpha + (1 - \alpha)\rho_0 \tag{4}$$

$$\mu = \mu_1 \alpha + (1 - \alpha)\mu_0 \tag{5}$$

where ρ is the fluid density, $\boldsymbol{U}$ – fluid velocity, t – time, p – pressure, μ – fluid kinematic viscosity, $\boldsymbol{F_g}$ – gravity force, $\boldsymbol{F_\sigma}$ – surface tension force, $\boldsymbol{F_E}$ – electrostatic force, α – volume fraction of fluid (index 1 is for liquid phase and 0 is for gas phase).

Poisson's Law and Gauss's Law:

$$\nabla \cdot (\varepsilon \nabla \varphi_E) = -\rho_E \tag{6}$$

where ε is the electric permittivity, φ_E – electric potential, ρ_E– volume charge density. This equation was obtained from Maxwell equations and allows the correlation between electric potential φ_E (Poisson's Law) and volume charge density – ρ_E.

Conservation of electric charge:

$$\frac{\partial \rho_E}{\partial t} + \nabla \cdot (\rho_E \boldsymbol{U}) = \nabla \cdot (\kappa \nabla \varphi_E) \tag{7}$$

where ρ_E is the volume charge density, t – time, $\boldsymbol{U}$ – fluid velocity, κ – electric conductivity and φ_E – electric potential. This equation describes convection and conduction of electric charge. The electric properties on the interface are calculated as harmonic averages:

$$\frac{1}{\kappa} = \frac{\alpha}{\kappa_1} + \frac{1 - \alpha}{\kappa_0} \tag{8}$$

$$\frac{1}{\varepsilon} = \frac{\alpha}{\epsilon_1} + \frac{1 - \alpha}{\epsilon_0} \tag{9}$$

The electric force $\boldsymbol{F_E}$ in Eq. (3), responsible for dragging the interface of the droplet and finally breaking it, can be described as divergence of electrostatic stress tensor $\boldsymbol{\Lambda}$:

$$\boldsymbol{\Lambda} = \varepsilon \left(\boldsymbol{EE} - \frac{\boldsymbol{E^2}}{2} \boldsymbol{i} \right) \tag{10}$$

Finally:

$$\boldsymbol{F_E} = \rho_E \boldsymbol{E} - \frac{1}{2} \boldsymbol{E^2} \nabla \varepsilon \tag{11}$$

where Λ is the electrostatic stress tensor, ε – electric permittivity, $\boldsymbol{E}$ – electric field strength, $\boldsymbol{i}$ – versor and $\boldsymbol{F_E}$ – electric force.

The surface tension force is defined as:

$$\boldsymbol{F_\sigma} = \sigma \boldsymbol{K} \frac{\partial \alpha}{\partial x_i} \tag{12}$$

where $\boldsymbol{F_\sigma}$ – surface tension force, σ – surface tension, α – volume fraction of liquid, x_i – one of dimensions, $\boldsymbol{K}$ – surface curvature.

In this case surface curvature is defined as:

$$\boldsymbol{K} = -\frac{\partial}{\partial x_i} \left(\frac{\dfrac{\partial \alpha}{\partial x_i}}{\left| \dfrac{\partial \alpha}{\partial x_i} \right|} \right) \tag{13}$$

2.2. Framework for model implementation

The mathematical model was implemented in OpenFOAM v. 7 (Jasak, 2009). The starting point was the *interFoam* solver, which is the numerical implementation of the standard VOF model. It solves Equations (1)–(5) and (12)–(13) (minus the electric strength term in Navier–Stokes equation). It was used for simulations without electric field. This solver has also an extended version, including dynamic mesh refinement – named *interDyMFoam* (Dynamic Mesh). It allows the user to increase the mesh density in a zone fulfilling some defined criteria. The new solver was named *ehdFoam* (and *ehdDyMFoam* if with dynamic mesh refinement). It solves all equations described above, from (1) to (13). It was used for simulations with electric field. However, in this work only static mesh was used, due to unsolved bug in the dynamic mesh refining algorithm in OpenFOAM.

2.3. Numerical implementation

The geometry of the standard computational domain, used for simulation with electric field, is depicted in Figure 1, for the variant with 0.44 mm nozzle inner diameter (in the second variant, the nozzle inner diameter equals 0.28 mm). For simulations without electric field, a simpler, shorter mesh was used.

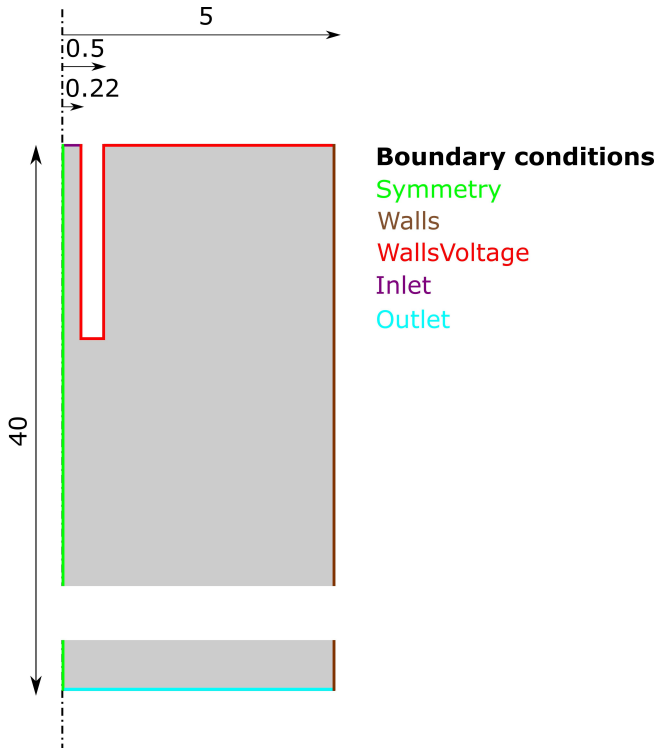

Fig. 1. Geometry and boundary conditions used for simulations with electric field

Geometry and mesh were created using a tool called *blockMesh* of toolbox OpenFOAM. The mesh was created from wedge shaped blocks in order to simulate the axisymmetrical domain. Therefore, the system is solved for one half of cross section, together with proper symmetry boundary conditions. The results are presented for the complete cross section, by mirroring the simulation outcome along the system symmetry axis.

The grid independence test was carried out at the beginning of simulations. 5 different mesh sizes were tested: 2900, 3800, 6500, 10500 and 11600 cells. The tested parameter was droplet breakup time. No strong influence of mesh size on breakup time was observed. The selected variant is the one with second

lowest number of cells. The choice was made based on two factors: selecting the lowest possible number of cells (to achieve the best time efficiency) while still maintaining good mesh quality. Selecting a small mesh was also required since simulations were run on a PC and not on a dedicated computing unit. The specifications of this machine are as follows: processor Intel® Core™ i7 3632QM (4 cores, 2.2 GHz), 8 GB RAM, 1 TB HDD.

The finally created meshes (for both nozzle diameters) had 3872 cells each. For the simulations with electric field, an extended domain was used, with a longer zone downstream the nozzle outlet (40 mm instead of 10 mm). This modified mesh had 13850 cells.

Mesh parameters were extracted using checkMesh tool. Maximum aspect ratio was 11.90, mesh non-orthogonality was 0 and maximum skewness was 0.33.

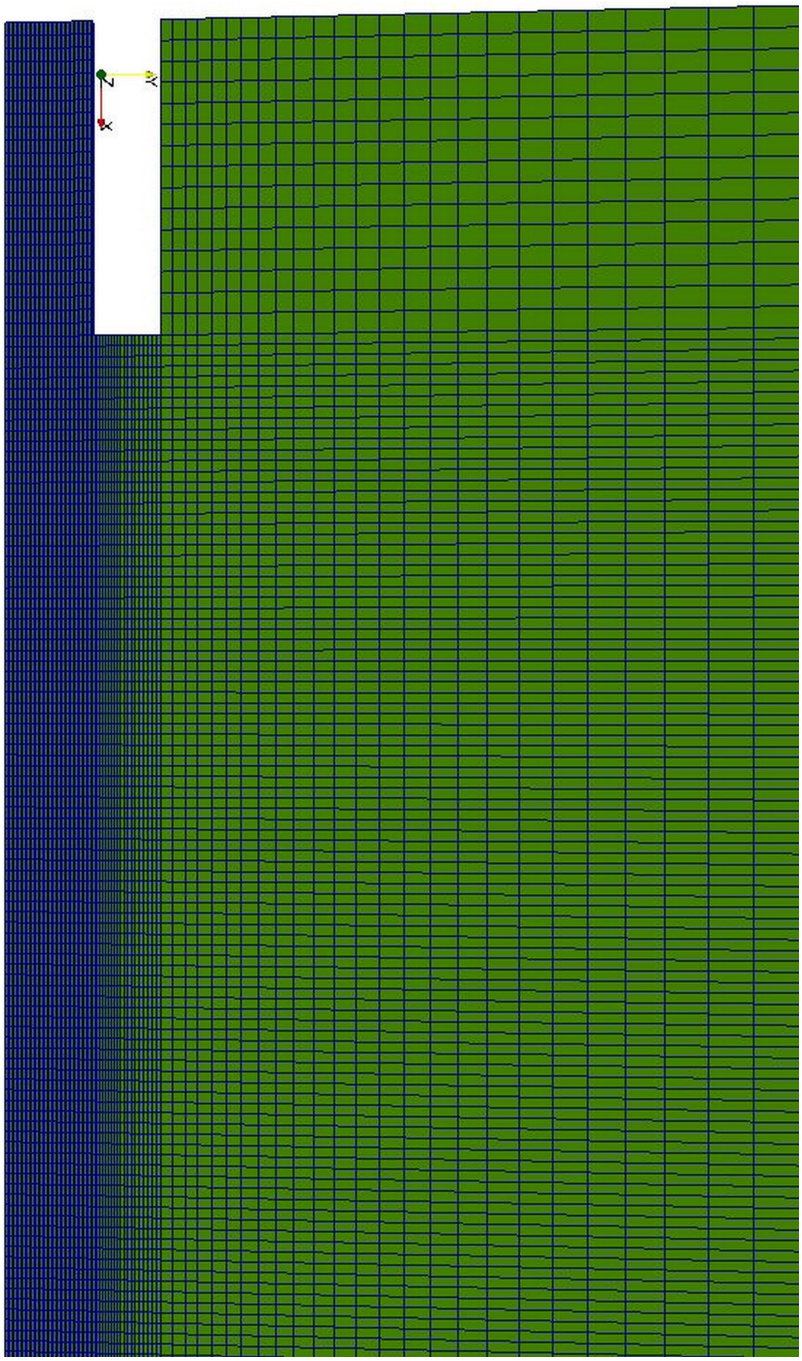

Fig. 2. Fragment of the computational mesh created in *blockMesh* tool

2.4. Boundary conditions and physicochemical properties

2.4.1. Boundary conditions

To start calculations, boundary conditions must be set up for velocity, pressure and volume fraction. If simulations include the electric field, then more information is needed – volume charge density and electric potential. All boundary conditions can be found in Table 1.

Table 1. Set of all boundary conditions used in calculations

	Velocity [m/s]	Pressure [Pa]	Liquid phase fraction [–]	Volume charge density [C/m^3]	Electric potential [V]
Symmetry	$\frac{\partial \boldsymbol{U}}{\partial x_i} = 0$	$\frac{\partial p}{\partial x_i} = 0$	$\frac{\partial \alpha}{\partial x_i} = 0$	$\frac{\partial \rho_E}{\partial x_i} = 0$	$\frac{\partial \varphi_E}{\partial x_i} = 0$
Walls	$\frac{\partial \boldsymbol{U}}{\partial x_i} = 0$	$\frac{\partial p}{\partial x_i} = 0$	$\frac{\partial \alpha}{\partial x_i} = 0$	$\rho_E = 0$	$\frac{\partial \varphi_E}{\partial x_i} = 0$
WallsVoltage	$\boldsymbol{U} = 0$	$\frac{\partial p}{\partial x_i} = 0$	$\frac{\partial \alpha}{\partial x_i} = 0$	$\rho_E = 0$	$\varphi_E = f(t)$
Inlet	$\boldsymbol{U} = (U_x, U_y, U_z)$	$\frac{\partial p}{\partial x_i} = 0$	$\alpha = 1$	$\rho_E = 0$	$\frac{\partial \varphi_E}{\partial x_i} = 0$
Outlet	$\frac{\partial \boldsymbol{U}}{\partial x_i} = 0$	$p = 0$	$\frac{\partial \alpha}{\partial x_i} = 0$	$\frac{\partial \rho_E}{\partial x_i} = 0$	$\varphi_E = 0$
Wedge +/−	periodic	periodic	periodic	periodic	periodic

At the outlet, a special boundary condition called *inletOutlet* was defined, which allow the special treatment of fluid reentering the domain. The top wall of the domain and wall of nozzle were set up with alternating electric potential boundary condition, described as follows:

$$\varphi_E = \varphi_{E\,\max}\, positive\ (\sin(2\pi f t)) \tag{14}$$

where φ_E – electric potential on wall, $\varphi_{E\,\max}$ – maximum electric potential, f – frequency of electric field oscillation and t – time. Equation (14) describes how the electric potential changes on the wall. It is introduced in order to mimic the alternating electric pulses from real-life experiment. It was implemented into OpenFOAM using a special tool named *groovyBC* (which allows to define more complex boundary conditions). The *positive* function returns the value of 1 for each positive argument, and 0 otherwise. It transforms the periodic sinus function into a rectangular function. As a result, the boundary condition presented in Eq. (14) allows to create a rectangular function with duty cycle of 50%, as used in laboratory experiments.

2.4.2. Simulation setup for cases without electric field

Twelve different sets of process parameters were created for the CFD simulations – for two different inner nozzle diameters (parameter code: D; either 0.28 or 0.44 mm), two sets of fluids (parameter code: M; water or alginate solution) and three different volumetric flow rates (parameter code: Q; 8, 5 or 16 ml/h). The flow rates were used to calculate the fluid inlet velocity for each set, using the known nozzle inner diameter. In Table 2, these velocities are summarized.

Table 2. Inlet velocities of liquid (calculated from volumetric flow rate and nozzle diameter)

Inner nozzle diameter [mm] (variant number)	Volumetric flow rate [ml/h] (variant number)	Calculated inlet velocity [m/s]
0.28 (D1)	8 (Q1)	0.081
	5 (Q2)	0.051
	16 (Q3)	0.162
0.44 (D2)	8 (Q1)	0.032
	5 (Q2)	0.021
	16 (Q3)	0.065

Two types of liquids were used – either water or an 2% aqueous solution of sodium alginate. In the simulations, both liquids were assumed to be Newtonian fluids. In Table 3, the physical properties of the fluids are listed.

Table 3. Density, kinematic viscosity, and surface tension coefficient of fluids used in simulations

Fluid	ρ [kg/m^3]	ν [m^2/s]	σ [N/m]
Water (M1)	1000	10^{-6}	0.07
Alginate solution (2%) (M2)	1012.5	$417 \cdot 10^{-6}$	0.06
Air	1	$15 \cdot 10^{-6}$	–

Each simulation was initialized with certain liquid phase fraction. The nozzle was filled with liquid and there was a small droplet hanging from the end of nozzle (for these regions $\alpha = 1$, the rest was $\alpha = 0$, at $t = 0$). The initial droplet was a perfect sphere with a diameter of $2d$ (twice the inner diameter of nozzle).

2.4.3. Simulation setup for cases with electric field

Calculations with electric field were carried out for two values of maximum electric potential $\varphi_{E\,\max}$ (parameter code: EP) and two values of frequency of oscillations f (parameter code: F). Parameter values are listed in Table 4.

Table 4. Variants of parameters for electric field boundary conditions

Variant	$\varphi_{E\,\max}$ (EP) [V]	f (F) [Hz]
1	10000	10
2	15000	50

Both liquids were treated as perfect dielectrics (Roghair et al., 2015). Very low values of electric conductivity were set, to avoid charge leak during droplet breakup. In Table 5, additional physical properties of fluids are listed.

Table 5. Additional physical properties of fluids for simulations with electric field

Fluid	κ_E [S/m]	ε_E [F/m]
Liquid	10^{-30}	$7.08 \cdot 10^{-10}$
Air	10^{-30}	$8.85 \cdot 10^{-12}$

2.4.4. Simulation setup for comparison with experimental data

The last step of simulations was the comparison of numerical results to ones obtained with the use of experimental setup. Experimental details are summarized in Table 6. The experiments were run with and without the electric field. The nozzle inner diameter was equal to 0.44 mm and its length was 7 mm. A nozzle concentric metal plate with 40 mm diameter was additionally used in experiments with the electric potential in order to provide a homogenous field, as this is also assumed in the mathematical model. Electric parameters were as follows: electric potential – 11 kV, frequency of oscillations – 5 Hz, duration of electrostatic impulse – 4 ms. The physical properties of glycerol solution taken for simulation are as follows. For 85% solution, the density was 1221.4 kg/m^3, viscosity was $89 \cdot 10^{-6}$ m^2/s. For 100% solution the density was 1261 kg/m^3, viscosity was $1119 \cdot 10^{-6}$ m^2/s. Surface tension coefficient was 0.06 N/m.

Table 6. Parameter sets used in experiments

Variant	Substance	Electric field	Liquid flow [ml/s]
1	Water	No	0.002778
2	Water	No	0.005556
3	Water	No	0.011111
4	Glycerol, c = 85%	No	0.001389
5	Glycerol, c = 85%	Yes	0.001389
6	Glycerol, c = 100%	No	0.001389
7	Glycerol, c = 100%	Yes	0.001389

2.5. Experimental

An electrostatic droplet generator with impulse voltage is schematically depicted in Figure 3.

The tested liquid is pumped by a syringe pump Alaris Asena (GH) to flow through a stainless steel nozzle with a given diameter. Droplets are formed at the nozzle tip and detach to the droplet collector below. The nozzle is connected to the positive end of a high voltage supply, coupled to a frequency modulator, whereas the collector is grounded. The setup enables to apply pulsed electric voltages to the nozzle and thus to charge flowing liquid in a controlled manner. Regulated electric parameters include: the applied voltage value φ_E (in the range 0–21 kV, stepwise), duration time of the voltage impulse t (in the range 1–9 ms, stepwise) and frequency of impulse application f (in the range 1–100 Hz, stepwise). The distance between the tip of the nozzle and the droplet generator can be regulated fluently. The droplet generator is accompanied by a camera and a DVD recorder, coupled to a video monitor, in order to record the process of droplet formation at the tip of the nozzle. The ambient temperature was equal to 25 °C and relative

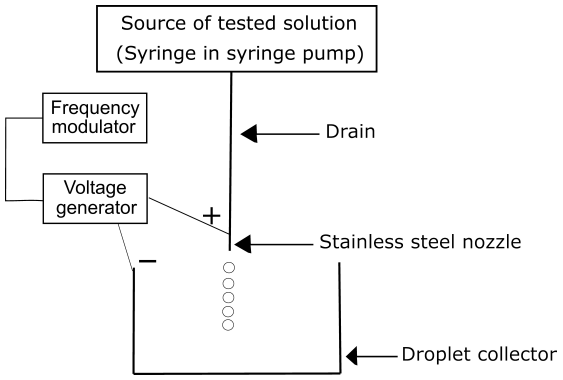

Fig. 3. Scheme of the electrostatic droplet generator with the impulse voltage generator

humidity was ca. 60% during all the experiments. All the measurements were done in triplicate. Finally, the droplet diameter was derived from measured time of a single droplet formation. The calculations were done according to the assumption that the droplet is spherical at the moment of detachment from the nozzle tip.

3. RESULTS AND DISCUSSION

3.1. Validation of CFD method

In order to test the accuracy of equations implemented to the solver, two numerical test cases were carried out, which were also used by Roghair et al. for validation of their EHD solver (Roghair et al., 2015). In the first test, in which two stationary liquids stacked vertically were simulated, the implementation of the Gauss's law and the Poisson's Law – the correlation between volume charge density and electric potential – was tested. The geometry was one-dimensional and the electric potential distribution was calculated. The obtained simulation results were compared with an analytical solution (see Fig. 4). In the second test case, the charge transport equation was tested for a 2D geometry, in which charge relaxation of an initial

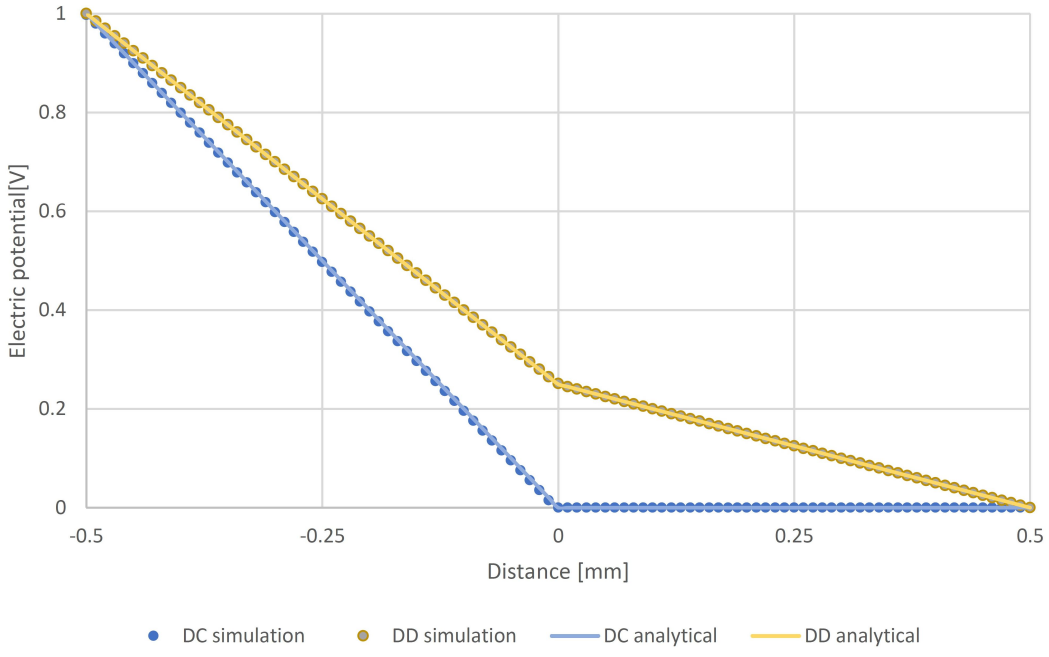

Fig. 4. Comparison of results of simulation with analytical solution for first validation case

charge distribution was observed. Also in this case, the numerical results were assessed by comparison with an analytical solution of the charge relaxation process (see Fig. 5). In all numerical test cases, CFD results were fully consistent with analytical solutions and with the validation results published by Roghair et. al. (2015).

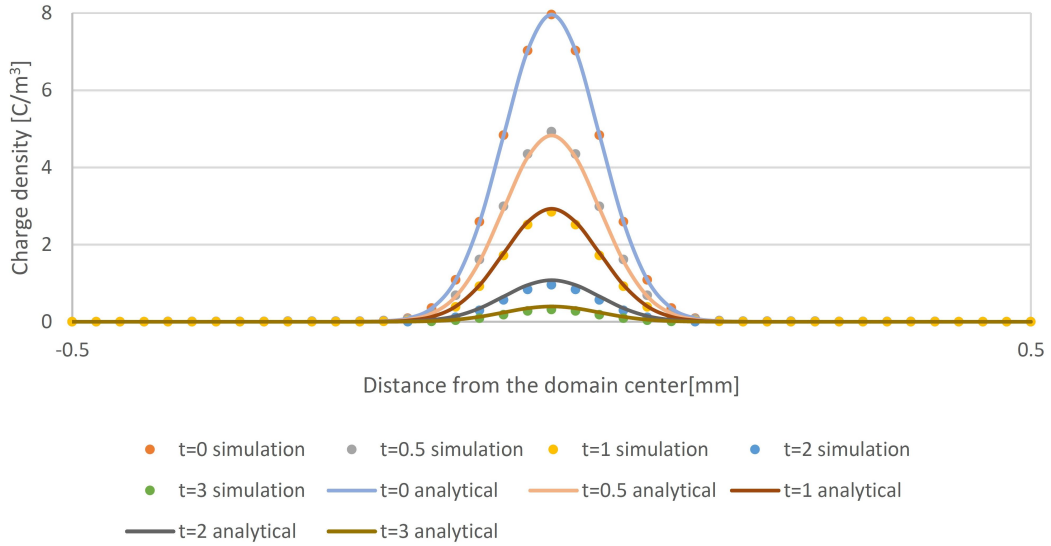

Fig. 5. Comparison of results of simulation with analytical solution for second validation case

3.2. CFD simulations of droplet generation process

3.2.1. Results without an electric field

The outcome of simulations will be presented using contour plots and tables with droplet breakup times. All the results will be discussed in further parts of this work. In Figure 6, exemplary CFD simulation results are presented. Contour plots of volume fraction show the process of droplet creation, growth and finally breakup. All post-processing (plots) were created using *ParaView* software.

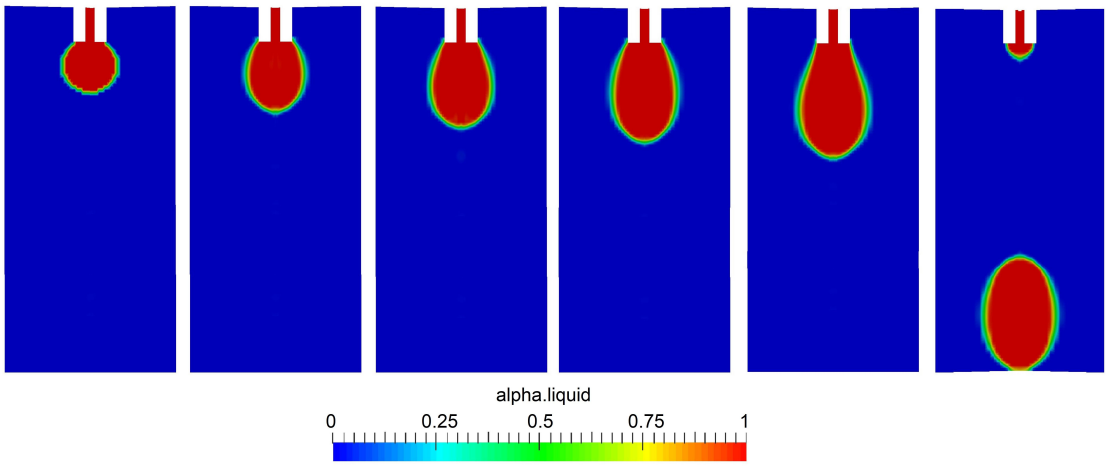

Fig. 6. Contour plots of liquid phase volume fraction in following time steps (each next plot is 0.25 s later than the previous one) – variant M1D1Q1

Simulations were carried out until four droplets were observed. Additionally, time intervals between each two subsequent droplets were calculated and the volume of the later droplet was calculated from the time interval. The breakup time of each first droplet differs from the other – it is related to simulation initialization with some volume of fluid in the nozzle.

For the M2 variant (sodium alginate solution), no droplet breakup was observed as it appeared that this solution is too viscous. Without support of the electric field, the liquid does not break into droplets – it stretches through the whole domain until it reaches the outlet. In Figure 7, two contour plots were presented for that case. Due to this kind of behavior, further calculations with sodium alginate, but without electric field, were ceased.

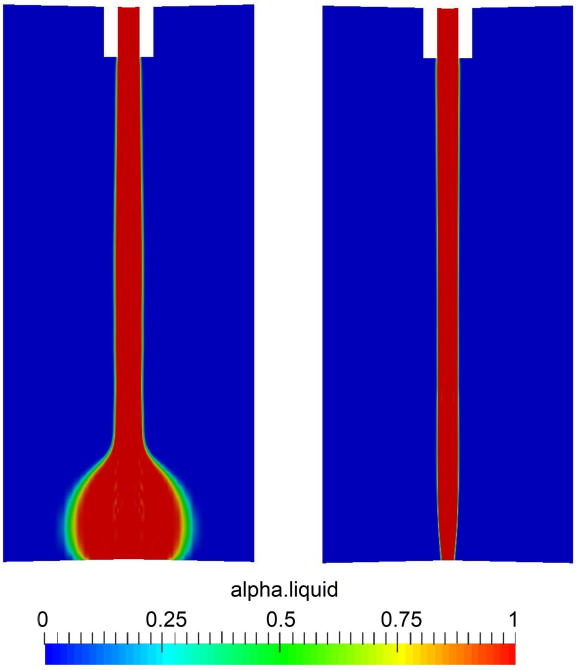

Fig. 7. Contour plot of volume fraction for 2% sodium alginate solution – droplet hanging on a liquid string and liquid along the whole domain – variant M2D1Q1

In Table 7, the estimated diameters of generated droplets are calculated, based on time intervals between subsequent droplets and the liquid flow rate.

Abbreviations used in following tables are as follows: M (type of liquid); D (nozzle diameter); Q (flow rate); F (electric field oscillation frequency) and EP (maximum electric potential).

Table 7. Calculated droplet diameters – case without electric field (M1, water)

Variant	Calculated droplet diameter [cm]			
	1	2	3	4
M1D1Q1	0.227	0.250	0.249	0.250
M1D1Q2	0.227	0.251	0.251	0.247
M1D1Q3	0.227	0.250	0.253	0.250
M1D2Q1	0.167	0.186	0.185	0.184

3.2.2. Results with the electric field

In Tables 8 and 9, the calculated droplet diameters are listed for both liquids used in the numerical study. There are some blank spaces in the tables – it is related to the instabilities of simulations for some sets of process parameters. Instead of regular droplet breakups, sudden “shots” of liquid were visible when

small portions of liquid were torn apart from currently forming droplets. This leads to occurrence of high velocities which in turn forces time step to go very low. If such a situation occurred, the simulation was stopped, as stable conditions with regular droplet breakups are generally desired.

Table 8. Calculated droplets diameters – case with the electric field (M1, water)

Variant	Calculated droplet diameter [cm]			
	1	2	3	4
Q1D1F1EP1	0.229			
Q1D1F2EP1	0.135	0.266		
Q1D1F1EP2	0.164	0.188	0.212	0.225
Q1D1F2EP2	0.113	0.165	0.187	0.225
Q1D2F1EP1	0.207			
Q1D2F2EP1	0.176	0.249		
Q1D2F1EP2	0.176	0.194		
Q1D2F2EP2	0.121	0.162	0.173	0.220
Q2D1F1EP1	0.235			
Q2D1F2EP1	0.140			
Q2D1F1EP2	0.140	0.121	0.161	0.188
Q2D1F2EP2	0.084	0.167	0.150	0.198
Q2D2F1EP1	0.232			
Q2D2F2EP1	0.252			
Q2D2F1EP2	0.141	0.189	0.189	0.206
Q2D2F2EP2	0.105	0.160	0.161	0.205
Q3D1F1EP1	0.219	0.237	0.238	
Q3D1F2EP1	0.242	0.205	0.271	0.333
Q3D1F1EP2	0.189	0.157	0.225	0.275
Q3D1F2EP2	0.155	0.197	0.180	0.223
Q3D2F1EP1	0.219	0.257	0.236	
Q3D2F2EP1	0.249	0.266		
Q3D2F1EP2	0.170	0.225	0.211	0.196
Q3D2F2EP2	0.128	0.192	0.171	0.179

In Figure 8, a few contour plots are presented for one variant of simulation. The first column contains plots of volume fraction. They show the following time steps of the process and how the fluid behaves during it. First, the inflow of liquid is visible, forming a droplet. Later it is stretched up to the moment of breakup (few millimeters away from the nozzle). The next column contains plots of electric potential.

Table 9. Calculated droplets diameters – case with the electric field (M2, alginate solution)

Variant	Calculated droplet diameter [cm]			
	1	2	3	4
Q1D1F1EP1	0.147	0.187	0.205	0.176
Q1D1F2EP1	0.113	0.177	0.212	0.187
Q1D1F1EP2	0.182	0.198	0.162	0.200
Q1D1F2EP2	0.212	0.206	0.164	0.222
Q1D2F1EP1	0.235	0.251	0.252	0.250
Q1D2F2EP1	0.238	0.256	0.255	0.256
Q1D2F1EP2	0.194	0.204	0.218	0.220
Q1D2F2EP2	0.220	0.225	0.233	0.227
Q2D1F1EP1	0.194	0.220	0.174	0.253
Q2D1F2EP1	0.153	0.214	0.132	0.260
Q2D1F1EP2	0.162	0.145	0.198	0.164
Q2D1F2EP2	0.151	0.221	0.216	0.232
Q2D2F1EP1	0.234	0.251	0.248	0.247
Q2D2F2EP1	0.240	0.254	0.256	0.259
Q2D2F1EP2	0.183	0.209	0.213	0.210
Q2D2F2EP2	0.203	0.226	0.224	0.223
Q3D1F1EP1	0.105	0.122	0.098	0.102
Q3D1F2EP1	0.159	0.215	0.130	0.176
Q3D1F1EP2	0.231			
Q3D1F2EP2	0.142	0.170	0.170	
Q3D2F1EP1	0.250	0.260	0.223	0.267
Q3D2F2EP1	0.258	0.264	0.263	0.263
Q3D2F1EP2	0.229	0.195	0.248	0.161
Q3D2F2EP2	0.250	0.249		

A regular, linear distribution of electric potential was observed, when there was a non-zero voltage applied (t = 2 s, t = 3.25 s) – otherwise the electric potential is zero in the whole domain (t = 3.1 s). The regular distribution of electric potential is interrupted by the droplet having different electric permittivity than air. The fourth column has contour plots of electric field strength acting on the interface. It is visible only in the moment of droplet breakup. It is worth noting that its values are very high – and thanks to that electric field can be used as a support for droplet creation. The last column contains drawing presenting velocities of fluids. In first two drawings the highest velocities are observed in the region of domain axis – it is related to oscillatory movement of droplet.

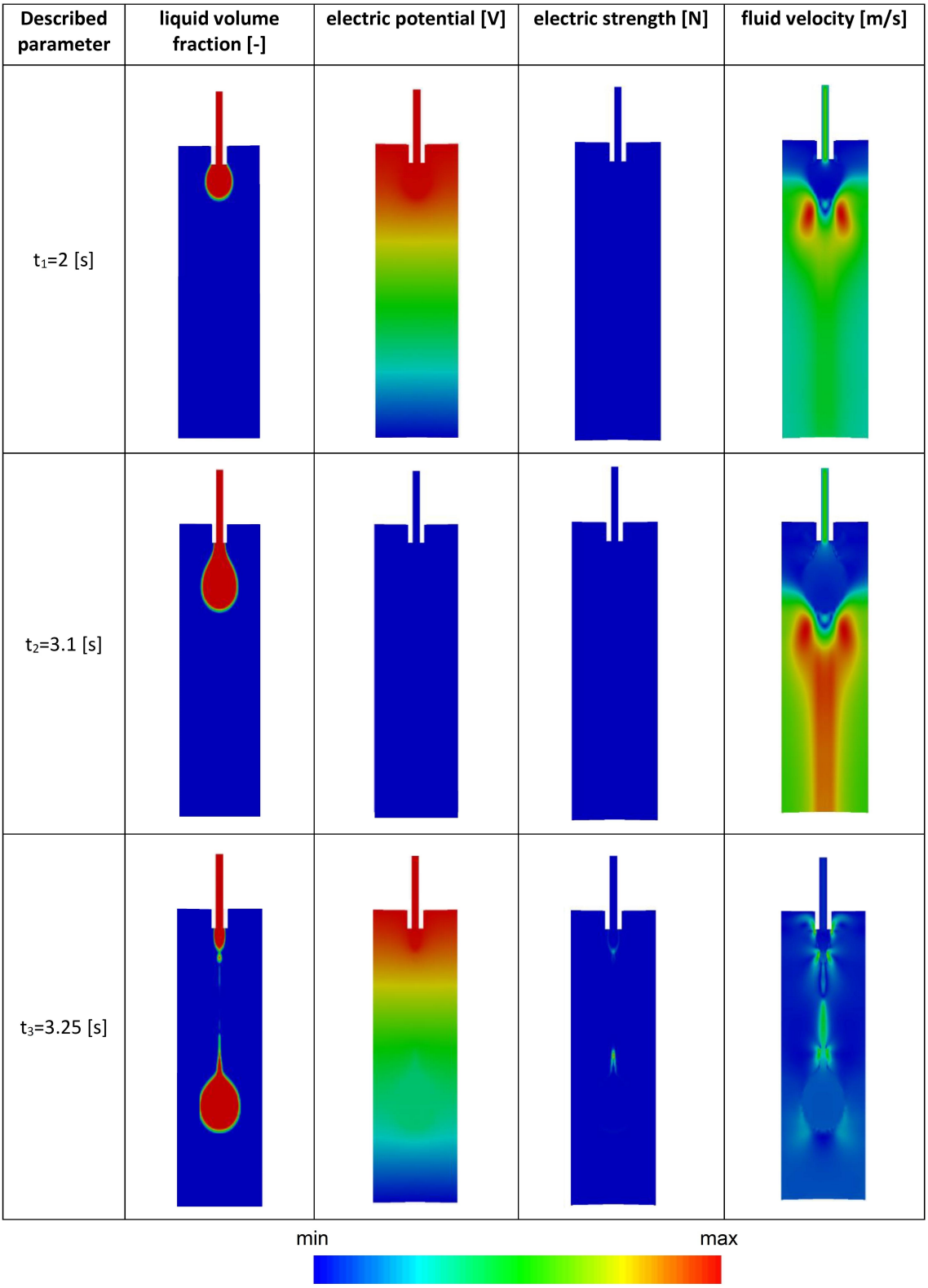

Fig. 8. Contour plots from simulation Q1D2F2EP1

3.3. Numerical simulations vs. experimental results

For the set of variants mentioned in Section 2.4.4. the corresponding numerical simulations were also conducted and droplet diameters were subsequently determined. The comparison of the obtained results is presented in Table 10.

Table 10. Comparison of numerical and experimental results

Variant	Substance	Electric field	Liquid flow [ml/s]	Averaged liquid velocity [m/s]	Numerical average droplet diameter [cm]	Experimental average droplet diameter [cm]	Relative difference [%]
1	Water	No	0.002778	0.005213	0.5064	0.2833	78.75
2	Water	No	0.005556	0.010426	0.2688	0.2868	–6.28
3	Water	No	0.011111	0.02085	0.2680	0.2845	–5.80
4	Glycerol, c = 85%	No	0.001389	0.002606	0.2537	0.2606	–2.65
5	Glycerol, c = 85%	Yes	0.001389	0.002606	0.2531	0.2239	13.04
6	Glycerol, c = 100%	No	0.001389	0.002606	0.2672	0.2449	9.11
7	Glycerol, c = 100%	Yes	0.001389	0.002606	0.2683	0.2275	17.93

Relative difference here is calculated as follows: the result from numerical solution subtracted from experimental value and then this difference is divided by experimental value. Positive values indicate that simulation overestimates the droplet diameter, negative ones mean underestimation.

Analyzing Table 10, it can be noticed that mathematical model in certain cases properly predicts experimental results (particularly variants no 2, 3, 4, 6). However, in variants with the electric field, some bigger discrepancies are observed (variants no 5 and 7). Besides, in case of discussed substances the model does not reflect changes in the droplet diameter caused by the presence of the electric field, though it does in case of alginate solution. The possible reason may be related to the impact of liquid viscosity on the course of the dispersion process. In addition, liquid flow also seems to be quite influential (both in terms of mean value and oscillations), as one may notice analyzing variants with water. The shape of the nozzle used in the experiments may also slightly differ from the nominal geometry used in the simulations, especially in the region of the outlet. Summarizing, one can conclude that the model gives promising results for the time being, though certainly it requires further elaboration and taking into account more variables (metal plate, different shapes of electric field etc.).

3.4. Discussion

3.4.1. Simulations without the electric field

Droplet generation in the absence of the electric field is driven by the effect of surface tension force and gravity force. The liquid flowing through the nozzle causes the droplet to grow and oscillate up to the moment of breakup. At this stage, it was observed that the lower the liquid velocity at inlet, the longer the time between two following droplets. This means that they fall when they reach certain volume (mass). Besides that, it was observed that nozzle with bigger diameter caused slightly longer interval between two following droplets.

The tested liquids have different viscosities and densities. During simulations it turned out that difference of viscosity had a big impact on the results. For a more viscous liquid, the droplets did not break up spontaneously. Other researchers have also encountered that problem (Bjørklund, 2009), some methods cannot generate droplets when viscosity is too high. The differences in densities were very low – around 1%, and as such it is assumable that it did not influence the results. The breakup time of the first droplet is always different from the others. It is related to initialization of simulation using an initial small volume of fluid at the nozzle outlet. Next droplets start from the same volume (left after droplet breaks free) so the following times are more stable.

3.4.2. Simulations with the electric field

The introduction of an oscillatory electric field in the droplet generation system changes the conditions and the outcome of the process significantly. When compared to the simulations without the electric field, the droplets oscillate more and are more elongated before breakup. Also, the frequency of the breakups is higher, leading to droplets with smaller diameters. Simulations were carried out until four droplets were observed. However, this was not possible for each set of parameters due to instabilities in calculations – very aggressive and rapid breakups occurred, which in turn led to very low time steps. These conditions show the limitation of the VOF-based mathematical model; on the other hand, usually they have to be avoided anyway for practical reasons.

These simulations were performed also for two different liquids. Water, when exposed to strong electric field was often ripped by small volumes from the main liquid stream, strong oscillations and elongation also occurred. Often during breakup, the water stream broke into a few droplets (not just one big). Besides, other interesting effect was noticed: the electric field broke the liquid but vanished so quickly that the liquid joined together as whole again (so, at this time, no droplet was formed). After few turns of such tearing the droplet was finally created. Simulations with alginate solution were much more regular. The calculations were stable. But the liquid stream became very elongated before breakup – up to the point where droplet "was created" outside the computational domain. Oscillations were weaker than in the previous case. Sometimes the liquid was elongated in direction perpendicular to axis – creating elliptic droplets rather than spherical ones. The breakups were regular and created droplets were, in general, bigger than for case with water. These differences between water and the sodium alginate solutions can be explained by the difference in liquid viscosity, as larger viscosity dampens local oscillations and contributes to stabilization of the flow. The influence of nozzle diameter on process was also tested. It turned out that for a nozzle with bigger diameter the droplets were bigger as well. This correlation was also proved in case without the electric field. The simulations for bigger diameter also resulted in more stable calculations. Another parameter changed in simulations was liquid flow rate. For smaller values the time required for creation of one droplet was higher, for bigger values it was lower. However, for the biggest flow rate used in simulations (Q3) the results were often irregular and chaotic – the velocities were too high. Such high values are not recommended if stable droplet generation conditions are desired.

It is evident that the addition of electric field influenced the process. Changing the strength of the electric field had bigger impact on the course of the droplet generation process than changing its frequency. Such high potential means faster droplet breakup, bigger elongation and oscillations of liquid. For cases with water and air high potential was stabilizing the simulations – they were more regular and no anomalies occurred. However, since the breakups were more frequent, droplets created had smaller volumes. The change of oscillation frequency slightly alters the oscillation of liquid before breakup. It seems that droplet hanging on nozzle oscillates stronger when frequency of oscillation of electric field is higher. The times of droplet breakups were compared as well. The results are much less regular then in the case without the electric field. What is interesting, regular times were achieved in most cases for alginate solution and bigger nozzle diameter. When water and air were fluids used for simulations, most stable results were achieved

for high electric potential variants. In general, the difference in time intervals between droplet breakups can be explained by the addition of the electric field.

The modeling approach presented in this work is generally consistent with the solutions presented in the literature. Regarding the hydrodynamics, certain flow regimes were identified, i.e. the droplet generation process occurs differently, depending on the process parameters (such as volumetric flow rate or electric potential applied). Similar to the results presented in this work, a strong influence of voltage on droplet formation was observed both in simulations and laboratory experiments, which seems to be the key factor for process control. Wei et al. (2013) reported that increase in applied voltage decreased droplet diameter. Most of the results of this work also behave that way, ones that do not are probably due to the domination of other parameters. Lastow and Balachandran (2006) noticed in his work that charge is mostly localized near the surface of liquid – a similar effect can be seen when observing electric strength in Figure 8. This strength, according to Equation (12), is directly related to volume charge density. Eberhardt et al. (2019) reported that viscosity or flow rate had no significant impact on mean droplet size. This is inconsistent with the results reported in this paper. This difference may be caused by different methods of generating droplets. Here, it was a volume of liquid ejected from nozzle and for Eberhardt it was a T-junction. Li and Zhang (2020) distinguished certain process regimes, depending on way the liquid flows out of nozzle. All of these were observed in this work as well. The first one is dripping, which is desired process outcome – the monodisperse droplet generation. The next one is dripping-jetting transition. The third is pure jetting – there is a thin jet of liquid at the end of which small droplets are generated. The last and the least desirable outcome is threading – there are no droplets and only a stable thread of liquid. The boundaries between these regimes were defined by Li and Zhang based on two dimensionless numbers – the capillary number (describing the ratio of viscous force to interfacial tension) and the electric capillary number (describing the ratio of electric force to interfacial tension). Increase in electric capillary number promotes transition from dripping regime into jetting. This was observed in this work as well – stronger electric field caused smaller droplets to appear, promoted jetting and sometimes even stopped the droplet generation process.

One of the aspects of the numerical study presented herein was the assessment of the role of viscosity on the course of the droplet generation process. Therefore, two liquids (water and 2% aqueous sodium alginate solution) strongly differing in viscosity and both treated as Newtonian fluids were selected. However, to fully represent the features of the sodium alginate solution, its viscoelastic properties (Belalia and Djelali, 2014) should be taken into account in the simulations, as they might influence the outcome of the process. For example, in the case of pendant drop formation of a viscoelastic fluid in the absence of the electric field, the process shows some similarity with results obtained for Newtonian fluids. However, a "bead-on-a-string" effect is observed, which stabilizes the process and reduces the number of potential secondary drops on primary drop breakup (Davidson et al., 2006; Tirtaatmadja et al., 2006). Other parameters which influence the process, especially in the presence of an electric field, include wettability and surface tension (He et al., 2017; Wei and Joo, 2022). These aspects of the droplet generation process, especially in terms of CFD simulations, will be studied in future work.

The primary aim of this work was to prove that CFD modeling can be successfully applied for numerical investigation of droplet generation for biomedical applications, including methods used for encapsulation of living cells. The model was successfully validated against our own experimental results. Moreover, the capability of the mathematical model was demonstrated and compared to similar modeling approaches in other fields of science and engineering. The presented modeling method constitutes a novel, versatile tool for numerical investigation of the droplet generation process and can be used for process and equipment optimization and for prediction of the key properties of droplets/capsules produced. The CFD modeling approach is a method complementary to the standard methods used in droplet generation and encapsulation studies for biomedical applications, namely extensive experimental studies. For example, Manojlovic et al. (2006) investigated experimentally the electrostatic extrusion process as a method for cell immobilization. Goosen et al. (1997) studied the production of alginate microbeads with and without somatic tissue

using an electrostatic droplet generator. In a similar work, Zhang and He (2009) performed a parametric study to find optimum ranges of spray voltage, flow rate, alginate concentration for producing alginate microcapsules by electrostatic spraying. Lewińska et al. (2012) investigated experimentally the operation of an electrostatic droplet generator with 3-coaxial-nozzle head for microencapsulation. Examples of studies, where some simple mathematical description supporting the analysis of experimental results was utilized, include the papers by Poncelet et al. (1994); Lewińska et al. (2004); Lewińska et al. (2008) and Kramek-Romanowska et al. (2019). In the last cited work, a factorial design was performed to assess the consequences of altering selected parameters in the process the impulse electrostatic droplet formation. However, none of these solutions is suited for performing numerical simulations of the whole process of droplet or microcapsule generation using the electric field. The modeling approach presented in this work overcomes these limitations. The mathematical model enables to perform simulations of the droplet generation process, giving an insight into the physics and transport phenomena being the foundation of the process. Thanks to the model, the number of experimental runs can be minimized, as the process can be investigated partly *in silica.* The model enables to predict the course of the process and to create flow maps with zones denoting different flow regimes. Moreover, it can be used for process optimization for finding the optimum set of process parameters depending on the desired outcome of the process. In this case, a limited experimental investigation can be performed for confirmation of the quality of droplets in the optimum conditions obtained from CFD modeling. The modeling method can also be used for finding optimum design of droplet and microcapsule generator without the need to actually manufacture the various design variants of the generators. The presented mathematical model can be extended by adding the description of mass and heat transfer effects, as well as by extension to more than two fluid phases, which in turn would enable to simulate the complete encapsulation process using the electrostatic impulse method in multi-nozzle systems (Lewińska et al., 2012).

4. CONCLUSIONS

A mathematical model describing the process of droplet generation using the electrostatic impulse method was developed, implemented into CFD software, and validated. The droplet generation process in a single nozzle system was investigated. The influence of various process parameters (type of liquid, nozzle diameter, flow rate and maximum electric potential) on the size of the resulting droplets was studied numerically. Other CFD simulation results were also compared with experimental data and a good agreement was found.

According to the numerical investigation of the droplet generation process, the following conclusions can be drawn:

- high liquid viscosity stabilizes the process, allows the creation of larger and more regular droplets;
- larger nozzle diameter allows formation of larger droplets;
- the liquid flow rate influences the process – optimization is required, too high values make droplets shapes irregular, too low make the process last very long;
- the applied electric potential has considerable influence on the process, a stronger electric field makes the liquid oscillate, elongate and break earlier (droplets of smaller volume);
- the second parameter of the electric field – frequency of oscillation – has much lower impact, higher values made liquid oscillate more (with higher frequency);
- the electric field (especially when electric potential is high) speeds up the process of droplet breakup and influences the resulting droplet volume, leading to smaller droplets;
- the phenomenon of concentration of electric charge at the air-liquid phase boundary in the presence of the electric field (and their mutual interaction) seems to be the key factor affecting the promotion of droplet generation.

The developed and validated mathematical model may be used for optimization of the process of droplet formation in the electric field for biomedical applications. Simulations allow the user to test the influence of virtually every single process parameter on the process, without the need of conducting expensive and time-consuming laboratory experiments. The presented model is going to be further developed by the addition of relations describing mass and heat transfer effects at the phase boundary (fluid evaporation and resultant cooling of liquid phase), advanced rheological models for the liquid phase, and by introducing additional concentric nozzles in order to simulate the complete encapsulation process using the electrostatic impulse method.

SYMBOLS

$\boldsymbol{E}$ electric field strength, V/m
$\boldsymbol{F_E}$ electric strength, N
$\boldsymbol{F_g}$ gravity force, N
$\boldsymbol{F_\mathrm{p}}$ inertia force, N
$\boldsymbol{F_\sigma}$ surface tension force, N
f frequency of oscillation, Hz
$\boldsymbol{i}$ versor, –
$\boldsymbol{n}$ surface normal vector, –
p pressure, Pa
t time,
$\boldsymbol{U}$ fluid velocity, m/s
x_i one of spatial dimensions, m

Greek symbols

α volume fraction of liquid phase, –
σ surface tension, N/m
ε electric permittivity, F/m
η dynamic viscosity of liquid, m^2/s
K surface curvature, –
κ electric conductivity, S/m
Λ electrostatic stress tensor, N/m^2
μ fluid dynamic viscosity, Pa s
ν fluid kinematic viscosity, m^2/s
ρ liquid density, kg/m^3
ρ_E volumetric charge density, C/m^3
φ_E electric potential, V

Subscripts

E index for electric quantities
i index for dimensions
0 index for gas phase
1 index for liquid phase

Abbreviations

D nozzle diameter in the variant code
EP voltage in the variant code
F frequency in the variant code
M type of liquid in the variant code
Q volumetric flow rate in the variant code

REFERENCES

Ahn B., Lee K., Louge R., Oh W.K., 2009. Concurrent droplet charging and sorting by electrostatic actuation. *Biomicrofluidics*, 3, 044102. DOI: 10.1063/1.3250303.

Allegretto G., Dobashi Y., Dixon K., Wyss J., Yao D., Madden J.D.W., 2018. Frequency domain analysis of droplet-based electrostatic transducers. *Smart Mater. Struct.*, 27, 074007. DOI: 10.1088/1361-665X/aac134.

Anugraha G., Madhumathi J., Prita P., Kaliraj P., 2015. Biodegradable poly-l-lactide based microparticles as controlled release delivery system for filarial vaccine candidate antigens, *Eur. J. Pharmacol.*, 747, 174–180. DOI: 10.1016/j.ejphar.2014.12.004.

Baskaran R., Lee C.J., Kang S.M., Oh Y., Jin S.E., Lee D.H., Yang S.G., 2018. Poly(lactic-co-glycolic acid) microspheres containing a recombinant parathyroid hormone (1-34) for sustained release in a rat model. *Indian J. Pharm. Sci.*, 80, 837–843. DOI: 10.4172/pharmaceutical-sciences.1000429.

Belalia F., Djelali N.E., 2014. Rheological properties of sodium alginate solutions. *Revue Roumaine de Chimie*, 59(2), 135–145.

Betancor L., Luckarift H.R., 2008. Bioinspired enzyme encapsulation for biocatalysis. *Trends Biotechnol*., 26, 566–572. DOI: 10.1016/j.tibtech.2008.06.009.

Bhatia S.R., Khattak S.F., Roberts S.C., 2005. Polyelectrolytes for cell encapsulation. *Curr. Opin. Colloid Interface Sci.*, 10, 45–51. DOI: 10.1016/j.cocis.2005.05.004.

Bjørklund E., 2009. The level-set method applied to droplet dynamics in the presence of an electric field. *Comput. Fluids*, 38, 358–369. DOI: 10.1016/j.compfluid.2008.04.008.

Bugarski B., Li Q., Goosen M.F.A., Poncelet D., Neufeld R.J., Vunjak G., 1994. Electrostatic droplet generation: Mechanism of polymer droplet formation. *AIChE J.*, 40, 1026–1031. DOI: 10.1002/aic.690400613.

Cárdenas-Bailón F., Osorio-Revilla G., Gallardo-Velázquez T., 2015. Microencapsulation of insulin using a W/O/W double emulsion followed by complex coacervation to provide protection in the gastrointestinal tract. *J. Microencapsulation*, 32, 308–316. DOI: 10.3109/02652048.2015.1017619.

Castellanos A. (Ed.), 1998. *Electrohydrodynamics*. Springer-Verlag Wien. DOI: 10.1007/978-3-7091-2522-9.

Chang T., 2019. ARTIFICIAL CELL evolves into nanomedicine, biotherapeutics, blood substitutes, drug delivery, enzyme/gene therapy, cancer therapy, cell/stem cell therapy, nanoparticles, liposomes, bioencapsulation, replicating synthetic cells, cell encapsulation/scaffold, biosorbent/immunosorbent haemoperfusion/plasmapheresis, regenerative medicine, encapsulated microbe, nanobiotechnology, nanotechnology. *Artif. Cells Nanomed. Biotechnol.*, 47, 997–1013. DOI: 10.1080/21691401.2019.1577885.

Chaves I.L., Duarte L.C., Coltro W.K.T., Santos D.A. 2020. Droplet length and generation rate investigation inside microfluidic devices by means of CFD simulations and experiments. *Chem. Eng. Res. Des.*, 161, 260–270. DOI: 10.1016/j.cherd.2020.07.015.

Darabi J., Rhodes C., 2006. CFD modeling of an ion-drag micropump. *Sens. Actuators, A*, 127, 94–103. DOI: 10.1016/j.sna.2005.10.051.

Davidson M.R., Harvie D.J., Cooper-White J.J., 2006. Simulations of pendant drop formation of a viscoelastic liquid. *Korea-Aust. Rheol. J.*, 18(2), 41–49.

de Vos P., 2017. Historical perspectives and current challenges in cell microencapsulation, In: Opara E.C. (Ed.), *Cell microencapsulation. Methods in Molecular Biology, vol 1479*. Humana New York, NY, 3–21. DOI: 10.1007/978-1-4939-6364-5_1.

Diel D., Lagranha V.L., Schuh R.S., Bruxel F., Matte U., Teixeiraa H.F., 2018. Optimization of alginate microcapsules containing cells overexpressing α-L-iduronidase using Box-Behnken design. *Eur. J. Pharm. Sci.*, 111, 29–37. DOI: 10.1016/j.ejps.2017.09.004.

Duan G., Haase M.F., Stebe K.J., Lee D., 2018. One-step generation of salt-responsive polyelectrolyte microcapsules via surfactant-organized nanoscale interfacial complexation in emulsions (SO NICE). *Langmuir*, 34, 847–853. DOI: 10.1021/acs.langmuir.7b01526.

Eberhardt A., Boŝković D., Loebbecke S., Panić S., Winter Y., 2019. Customized design of scalable microfluidic droplet generators using step-emulsification methods. *Chem. Eng. Technol.*, 10:2195–2201. DOI: 10.1002/ceat.201900143.

Ferreira I.S., Bettencourt A., Betrisey B,. Gonçalves L.M.D., Trampuz A., Almeida A., 2015. Improvement of the antibacterial activity of daptomycin-loaded polymeric microparticles by Eudragit RL 100: An assessment by isothermal microcalorimetry. *Int. J. Pharm.*, 485, 171–182. DOI: 10.1016/j.ijpharm.2015.03.016.

Ganesh G.N.K., Chopra V., Karri V.V.S.R., Koundinya S.K., Kumar R.S., Arun R., 2018. Development and characterization of core–shell nanoparticles for anticancer therapy. *Adv. Sci. Lett.*, 24, 5768–5777(10). DOI: 10.1166/asl. 2018.12194.

Goosen M.F.A., Al-Ghafri A.S., El Mardi O., Al-Belushi M.I.J., Al-Hajri H.A., Mahmoud E.S.E., Consolacion E.C., 1997. Electrostatic droplet generation for encapsulation of somatic tissue: Assessment of high-voltage power supply. *Biotechnol. Progr.*, 13, 497–502. DOI: 10.1021/bp970020d.

He B., Yang S., Qin Z., Wen B., Zhang C., 2017. The roles of wettability and surface tension in droplet formation during inkjet printing. *Sci. Rep.*, 7, 11841. DOI: 10.1038/s41598-017-12189-7.

Hirt C.W., Nichols B.D., 1981. Volume of fluid (VOF) method for the dynamics of free boundaries. *J. Comput. Phys.*, 39, 201–225. DOI: 10.1016/0021-9991(81)90145-5.

Hu S., de Vos P., 2019. Polymeric approaches to reduce tissue responses against devices applied for islet-cell encapsulation. *Front. Bioeng. Biotechnol.*, 7, 134. DOI: 10.3389/fbioe.2019.00134.

Hunkeler D., Rehor A., Ceausoglu I., Schuldt U., Canaple L., Bernard P., Renken A., Rindisbacher L., Angelova N., 2001. Objectively assessing bioartificial organs. *Ann. N. Y. Acad. Sci.*, 944, 456–471. DOI: 10.1111/j.1749-6632.2001.tb03855.x.

Hyerim K., Chaewon B., Yun-Min K., Won-Gun K., Kangwon L., Min HP., 2019. Mesenchymal stem cell 3D encapsulation technologies for biomimetic microenvironment in tissue regeneration. *Stem Cell Res. Ther.*, 10, 51. DOI: 10.1186/s13287-018-1130-8.

IUPAC, 1997. *Compendium of Chemical Terminology, 2nd ed. (the "Gold Book")*. Compiled by McNaught A.D., Wilkinson A. Blackwell Scientific Publications, Oxford. XML on-line corrected version: http://goldbook.iupac.org (2006).

Jasak H., 2009. OpenFOAM: Open source CFD in research and industry. *Int. J. Nav. Archit. Ocean Eng.*, 1, 89–94. DOI: 10.3744/JNAOE.2009.1.2.089.

Kobayashi I., Vladisavljević G.T., Uemura K., Nakajima M., 2011. CFD analysis of microchannel emulsification: Droplet generation process and size effect of asymmetric straight flow-through microchannels. *Chem. Eng. Sci.*, 66, 5556–5565. DOI: 10.1016/j.ces.2011.07.061.

Köster S., Angilè F.E., Duan H., Agresti J.J., Wintner A., Schmitz C., Rowat A.C., Merten C.A., Pisignano D., Griffiths A.D., Weitz D.A., 2008. Drop-based microfluidic devices for encapsulation of single cells. *Lab Chip*, 8, 1110–1115. DOI: 10.1039/B802941E.

Kramek-Romanowska K., Grzeczkowicz M., Korycka P., Lewińska D., 2019. A factorial design for assessment of the effect of selected process variables on the impulse electrostatic droplet formation, In: Korbicz J., Maniewski R., Patan K., Kowal M. (Eds.), *Current trends in biomedical engineering and bioimages analysis*. PCBEE 2019. Advances in Intelligent Systems and Computing, 1033. Springer, Cham. DOI: 10.1007/978-3-030-29885-2_30.

Krishnan R., Alexander M., Robles L., Foster III C.E., Lakey J.R.T., 2014. Islet and stem cell encapsulation for clinical transplantation. *Review Diabetic Stud.*, 11, 84. DOI: 10.1900/RDS.2014.11.84.

Lastow O., Balachandran W., 2006. Numerical simulation of electrohydrodynamic (EHD) atomization. *J. Electrostat.*, 64, 850–859. DOI: 10.1016/j.elstat.2006.02.006.

Lewińska D., Bukowski J., Kożuchowski M., Kinasewicz A., Weryński A., 2008. Electrostatic microencapsulation of living cells. *Biocybern. Biomed. Eng.*, 28, 69–84.

Lewińska D., Chwojnowski A., Wojciechowski C., Kupikowska-Stobba B., Grzeczkowicz M., Weryński A., 2012. Electrostatic droplet generator with 3-coaxial-nozzle head for microencapsulation of living cells in hydrogel covered by synthetic polymer membranes. *Sep. Sci.Technol.*, 47, 463–469. DOI: 10.1080/01496395.2011.617350.

Lewińska D., Rosiński S., Weryński A., 2004. Influence of process conditions during impulsed electrostatic droplet formation on size distribution of hydrogel beads. *Artif. Cells, Blood Substitues, Biotechnol.*, 32, 41–53. DOI: 10.1081/BIO-120028667.

Li L., Zhang C., 2020. Electro-hydrodynamics of droplet generation in a co-flowing microfluidic device under electric control. *Colloids Surf., A*, 586, 124258. DOI: 10.1016/j.colsurfa.2019.124258.

Lim F., Sun A.M., 1980. Microencapsulated islets as bioartificial endocrine pancreas. *Science*, 210, 908–910. DOI: 10.1126/science.6776628.

Liu H., Cui S.W., Chen M., Ii Y., Liang R., Xu F., Zhong F., 2019. Protective approaches and mechanisms of microencapsulation to the survival of probiotic bacteria during processing, storage and gastrointestinal digestion: A review. *Crit. Rev. Food Sci. Nutr.*, 59, 2863–2878. DOI: 10.1080/10408398.2017.1377684.

López-Herrera J.M., Popinet S., Herrada M.A., 2011. A charge-conservative approach for simulating electrohydrodynamic two-phase flows using volume-of-fluid. *J. Comput. Phys.*, 230, 1939–1955. DOI: 10.1016/j.jcp.2010.11.042.

Madene A., Jacquot M., Scher J., Desobry S., 2006. Flavour encapsulation and controlled release–a review. *Int. J. Food Sci. Technol.*, 41, 1–21. DOI: 10.1111/j.1365-2621.2005.00980.x.

Manjula K., Bhagath Y.B., 2017. New generation functional foods-a prospectus on processing technology assistance in development and production – a review. *Carpathian J. Food Sci. Technol.*, 9(2), 64-76.

Manojlovic V., Djonlagic J., Obradovic B., Nedovic V., Bugarski B., 2006. Immobilization of cells by electrostatic droplet generation: a model system for potential application in medicine. *Int. J. Nanomedicine*, 1, 163–171. DOI: 10.2147/nano.2006.1.2.163.

Osswald C.R., Kang-Mieler J.J., 2016. Controlled and extended in vitro release of bioactive anti-vascular endothelial growth factors from a microsphere-hydrogel drug delivery system. *Curr. Eye Res.*, 41, 1216–1222. DOI: 10.3109/02713683.2015.1101140.

Papadimitriou V.A., Kruit S.A., Segerink L.I., Eijkel J.C.T., 2020. Droplet encapsulation of electrokinetically focused analytes without loss of resolution. *Lab Chip*, 20, 2209–2217. DOI: 10.1039/D0LC00191K.

Picot A., Ongmayeb G., Poncelet D., 2015. Microencapsulation as an innovative tool to enhance the functions and properties of bioactive ingredients. *Agro Food Industry Hi-Tech*, 26(2), 38–41.

Pierre A.C., 2004. The sol-gel encapsulation of enzymes. *Biocatal. Biotransform.,* 22, 145–170. DOI: 10.1080/10242420412331283314.

Plog J., Jiang Y., Pan Y., Yarin A.L., 2020. Electrostatic charging and deflection of droplets for drop-on-demand 3D printing within confinements. *Addit. Manuf.*, 36, 101400. DOI: 10.1016/j.addma.2020.101400.

Poncelet D., Neufeld R., Bugarski B., Amsden B.G., Zhu J., Goosen M.F.A., 1994. A parallel plate electrostatic droplet generator: parameters affecting microbead size. *Appl. Microbiol. Biotechnol.*, 42, 251–255. DOI: 10.1007/BF00902725.

Prüsse U., Bilancetti L., Bučko M., Bugarski B., Bukowski J., Gemeiner P., Lewińska D., Manojlovic V., Massart B., Nastruzzi C., Nedovic V., Poncelet D., Siebenhaar S., Tobler L., Tosi A., Vikartovská A., Vorlop K-D., 2008. Comparison of different technologies for alginate beads production. *Chem. Pap.*, 62, 364–374. DOI: 10.2478/s11696-008-0035-x.

Rahman K., Ko J.B., Khan S., Kim D.S., Choi K.H., 2010. Simulation of droplet generation through electrostatic forces. *J. Mech. Sci. Technol.*, 24, 307–310. DOI: 10.1007/s12206-009-1149-y.

Rakoczy R., Kordas M., Markowska-Szczupak A., Konopacki M., Augustyniak A., Jabłońska J., Paszkiewicz O., Dubrowska K., Story G., Story A., Ziętarska K., Sołoducha D., Borowski T., Roszak M., Grygorcewicz B., Dołęgowska B., 2021. Studies of a mixing process induced by a rotating magnetic field with the application of magnetic particles. *Chem. Process Eng.*, 42, 157–172. DOI: 10.24425/cpe.2021.138922.

Rathore S., Desai P.M., Liew C.V., Chan L.W., Heng P.W.S., 2013. Microencapsulation of microbial cells. *J. Food Eng.*, 116, 369–381. DOI: 10.1016/j.jfoodeng.2012.12.022.

Roghair I., Musterd M., van den Ende D., Kleijn C., Kreutzer M., Mugele F., 2015. A numerical technique to simulate display pixels based on electrowetting. *Microfluid. Nanofluid.*, 19, 465–482. DOI: 10.1007/s10404-015-1581-5.

Shahidi F., Han X.-Q., 1993. Encapsulation of food ingredients. *Crit. Rev. Food Sci. Nutr.*, 33, 501–547. DOI: 10.1080/10408399309527645.

Tirtaatmadja V., McKinley G.H., Cooper-White J.J., 2006. Drop formation and breakup of low viscosity elastic fluids: Effects of molecular weight and concentration. *Phys. Fluids*, 18, 043101. DOI: 10.1063/1.2190469.

Tomar G., Gerlach D., Biswas G., Alleborn N., Sharma A., Durst F., Welch S.W.J., Delgado A., 2007. Two-phase electrohydrodynamic simulations using a volume-of-fluid approach. *J. Comput. Phys.*, 227, 1267–1285. DOI: 10.1016/j.jcp.2007.09.003.

Vaithilingam V., Kollarikova G., Qi M., Lacik I., Oberholzer J., Guillemin G.J., Tuch B.E., 2011. Effect of prolonged gelling time on the intrinsic properties of barium alginate microcapsules and its biocompatibility. *J. Microencapsulation*, 28, 499–507. DOI: 10.3109/02652048.2011.586067.

Vaithilingam V., Tuch B.E., 2011. Islet transplantation and encapsulation: an update on recent developments. *Rev. Diabetic Stud.*, 8, 51–67. DOI: 10.1900/RDS.2011.8.51.

Vakilinezhad M.A., Alipour S., Montaseri H., 2018. Fabrication and *in vitro* evaluation of magnetic PLGA nanoparticles as a potential Methotrexate delivery system for breast cancer. *J. Drug Delivery Sci. Technol.*, 44, 467–474. DOI: 10.1016/j.jddst.2018.01.002.

Vemmer M., Patel A.V., 2013. Review of encapsulation methods suitable for microbial biological control agents. *Biol. Control*, 67, 380–389. DOI: 10.1016/j.biocontrol.2013.09.003.

Wei B.S., Joo S.W., 2022. The effect of surface wettability on viscoelastic droplet dynamics under electric fields. *Micromachines*, 13, 580. DOI: 10.3390/mi13040580.

Wei W., Gu Z., Wang S., Zhang Y., Lei K., Kase K., 2013. Numerical simulation of the cone–jet formation and current generation in electrostatic spray—modeling as regards space charged droplet effect. *J. Micromech. Microeng.*, 23, 015004. DOI: 10.1088/0960-1317/23/1/015004.

Wu M., Sammons P.M., Barton K., 2017. Numerical modeling of high resolution electrohydrodynamic jet printing using OpenFOAM. *Solid Freeform Fabrication 2017: Proceedings of the 28th Annual International Solid Freeform Fabrication Symposium – An Additive Manufacturing Conference*, 1176–1190.

Xia Y., Reboud J.-L., 2019. Hydrodynamic and electrostatic interactions of water droplet pairs in oil and electrocoalescence. *Chem. Eng. Res. Des.*, 144, 472–482. DOI: 10.1016/j.cherd.2019.02.012.

Xie Y., Bos D., de Vreede L.J., de Boer H.L., van der Meulen M.-J., Versluis M., Sprenkels A.J., van den Berg A., Eijkle J.C.T., 2014. High-efficiency ballistic electrostatic generator using microdroplets. *Nat. Commun.*, 5, 3575. DOI: 10.1038/ncomms4575.

Yaakov N., Mani K.A., Felfbaum R., Lahat M., Da Costa N., Belausov E., Ment D., Mechrez G., 2018. Single cell encapsulation via pickering emulsion for biopesticide applications. *ACS Omega*, 3, 14294–14301. DOI: 10.1021/acsomega.8b02225.

Zhai P., Chen X.B., Schreyer D.J., 2015. PLGA/alginate composite microspheres for hydrophilic protein delivery. *Mater. Sci. Eng., C*, 56, 251–259. DOI: 10.1016/j.msec.2015.06.015.

Zhang W., He X., 2009. Encapsulation of living cells in small (~100 μm) alginate microcapsules by electrostatic spraying: a parametric study. *J. Biomech Eng.*, 131, 074515. DOI: 10.1115/1.3153326.

Received 08 November 2021
Received in revised form 06 June 2022
Accepted 08 June 2022